JOURNAL OF ENZYME INHIBITION AND MEDICINAL CHEMISTRY
2022, VOL. 37, NO. 1, 1514–1526
https://doi.org/10.1080/14756366.2022.2077731

Taylor & Francis
Taylor & Francis Group

RESEARCH PAPER

Design, synthesis, and biological evaluation of triazole-pyrimidine-methylbenzonitrile derivatives as dual A_{2A}/A_{2B} adenosine receptor antagonists

Zhi Li[a], Lijuan Kou[a], Xinzhen Fu[a], Zeping Xie[a], Maolei Xu[a], Lin Guo[a], Tiantian Lin[b], Shizhou Gong[b], Shumin Zhang[a] and Ming Liu[a]

[a]School of Pharmacy, Binzhou Medical University, Yantai, China; [b]Luye Pharma Group, Yantai, China

ABSTRACT

A series of novel dual A_{2A}/A_{2B} AR antagonists based on the triazole-pyrimidine-methylbenzonitrile core were designed and synthesised. The A_{2A} AR antagonist cAMP functional assay results were encouraging for most target compounds containing quinoline or its open-ring bioisosteres. In addition, compound **7i** displayed better inhibitory activity on A_{2B} AR (IC_{50} 14.12 nM) and higher potency in IL-2 production than AB928. Moreover, molecular docking studies were carried out to explain the rationality of molecular design and the activity of compound **7i**. Further studies on **7f** and **7i** revealed good liver microsomes stabilities and acceptable *in vivo* PK profiles. This study provides insight into the future development of dual A_{2A}/A_{2B} AR antagonists for cancer immunotherapy.

ARTICLE HISTORY
Received 17 January 2022
Revised 15 April 2022
Accepted 10 May 2022

KEYWORDS
Dual A_{2A}/A_{2B} adenosine receptor antagonists; quinoline; methylbenzonitrile; T cell activation; pharmacokinetics

1. Introduction

Adenosine is one of the most important signalling molecules in the human body, and it exerts its effects through G-protein coupled receptors, including A_1, A_{2A}, A_{2B}, and A_3 adenosine receptors (ARs)[1–3]. Upon activation by adenosine, A_{2A} AR and A_{2B} AR promote adenylyl cyclase (AC) activation and subsequent cyclic AMP (cAMP) production[4,5]. Elevated intracellular cAMP in T cells will result in T cell anergy by reducing its proliferation, maturation, cytokine production (e.g., IL-2), and tumour-killing activity[6–8]. The cell cytotoxicities of natural killer cells, dendritic cells, or macrophages are inhibited by this pathway as well[9–11]. In the tumour microenvironment (TME), the level of extracellular adenosine is higher than that of normal tissue, leading to immune evasion[4,12,13]. A_{2A} and A_{2B} ARs are widely considered critical to the immune functions of adenosine. The relevance of A_2 receptors in tumour immunotherapy has stimulated the development of various selective antagonists for these receptors[14–19].

In recent years, the discovery and translation of A_2 AR antagonists from the bench to bedside for cancer immunotherapy have made significant progress, with some selective A_2 AR antagonists entering clinical trials either alone or in combination with other immunotherapies (Figure 1)[1,20–23]. Previous studies mostly focussed on the discovery of inhibitors against the A_{2A} receptor. ZM241385 (Figure 1) is a very potent and selective A_{2A} AR antagonist developed by the AstraZeneca Group[24]. It can inhibit and delay tumour growth significantly[25]. The structural analysis of A_{2A} AR bound to ZM241385 confirmed the π–π stacking interaction with Phe168 and hydrogen bonds (H bonds) with Asn253 established by inhibitors were beneficial to improving the binding ability to the A_{2A} receptor, and this finding has facilitated the discovery of novel AR antagonists[26–29]. For example, the A_{2A} AR inhibitor CPI-444 (Figure 1) developed by Corvus Pharmaceuticals is considered to have a similar target binding form to ZM241385 and it is currently in a phase 1b/2 trial for the treatment of renal cell cancer[1,2,30].

Since the A_{2B} receptor is also important in adenosine signal transduction, especially in cells of myeloid origin, a dual A_{2A}/A_{2B} AR antagonist usually exhibits better inhibition effects[9,18,31,32]. Azolopyrimidines (e.g., compound A in Figure 2) were first disclosed by Arcus Biosciences as A_{2A}R antagonists[33]. However, AB928 contains methylbenzonitrile, instead of the furan fragment of compound A, and it can inhibit A_{2A} AR and A_{2B} AR with similar potencies and outperform others in preclinical testing[22]. In 2019, Selvita Group published a patent on imidazo[1,2-a]pyrazines for the treatment of tumour-related disorders[34]. Among these imidazo[1,2-a]pyrazines, SEL330-639 containing the quinoline structure was confirmed to be a dual A_{2A}/A_{2B} receptor antagonist with nanomolar potency[9]. Through the structure–activity relationship of the above two compounds, methylbenzonitrile and quinoline structures may be advantageous scaffolds to obtain potent dual A_{2A}/A_{2B} AR antagonists. Incyte Corporation developed two types of A_{2A}/A_{2B} inhibitors (Figure 2, compounds B and C)[35,36]. Compounds containing benzonitrile structure or quinoline analogues also showed good inhibitory activities on both of these two receptors. Thus, we introduced quinoline or its open-ring bioisosteres to the structure of AB928 to develop new dual A_{2A}/A_{2B} AR antagonists. Herein, a series of novel A_2 AR antagonists containing triazole-pyrimidine-methylbenzonitrile core were designed and synthesised (Figure 2, compounds D). Their potential inhibitory activities to A_{2A} or A_{2B} ARs were further investigated by cAMP functional assay and T cell activation assay. In addition, the representative compound **7i** was subjected to molecular docking studies to reveal the binding behaviour. Moreover,

CONTACT Shumin Zhang shumin_zhang@outlook.com; Ming Liu ytliuming@163.com School of Pharmacy, Binzhou Medical University, Yantai 264003, China

Supplemental data for this article is available online at https://doi.org/10.1080/14756366.2022.2077731.

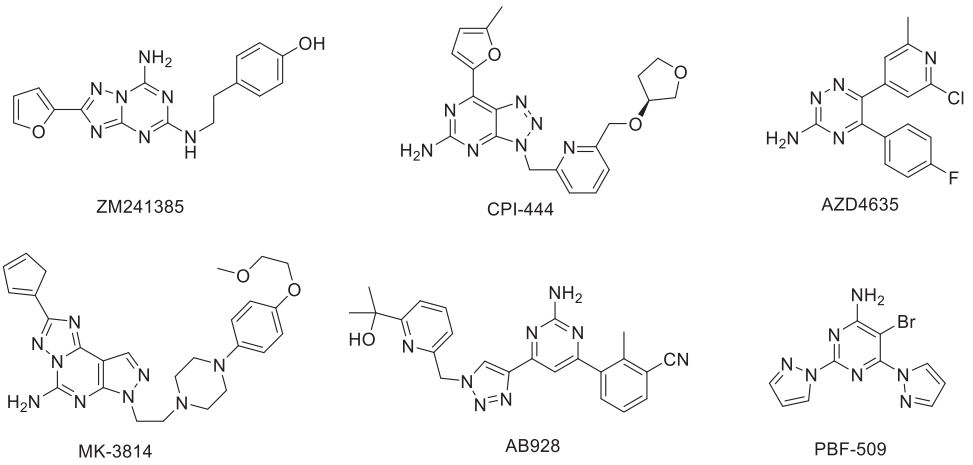

Figure 1. Chemical structures of A_2 adenosine receptor antagonists.

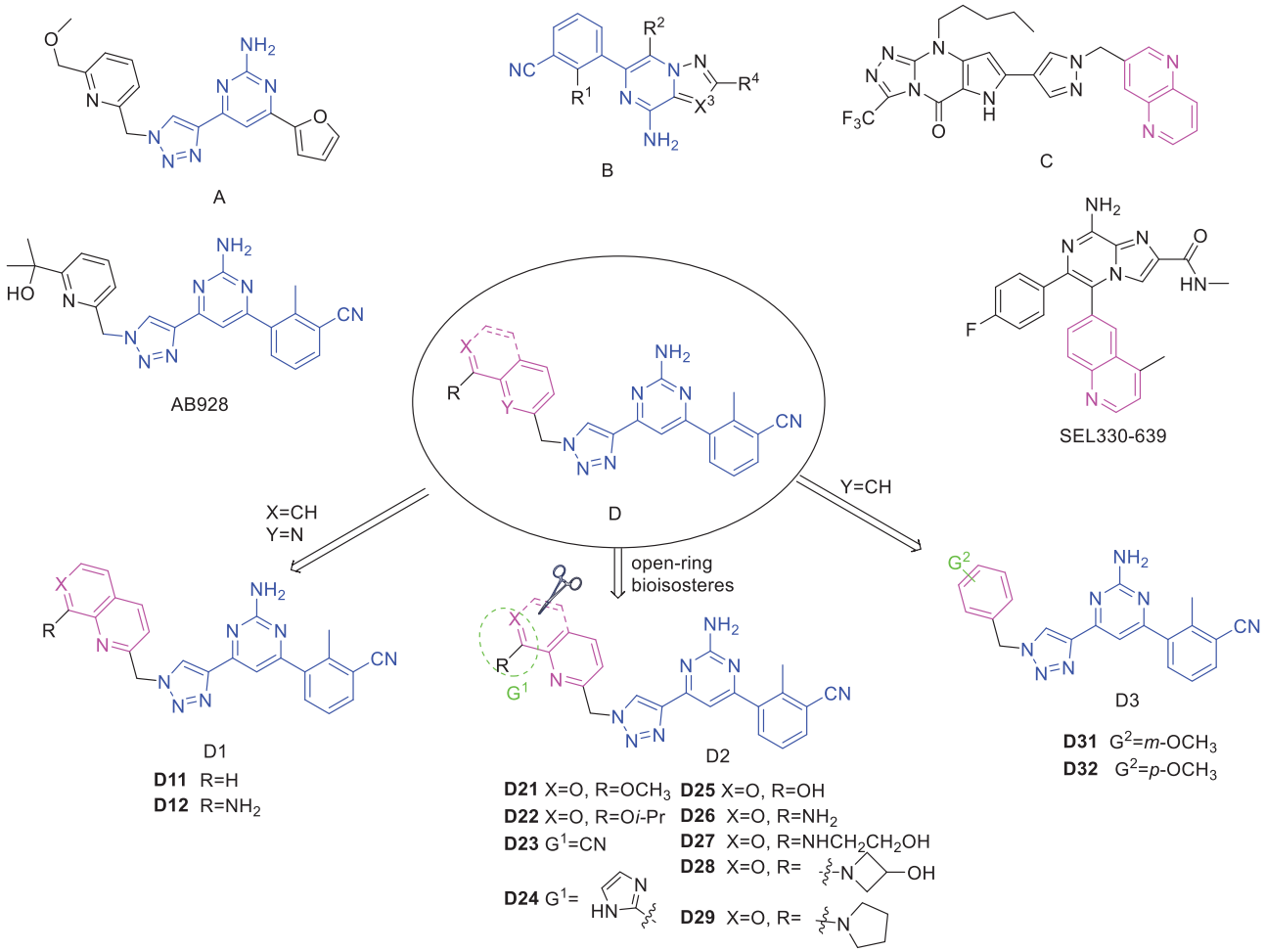

Figure 2. Design of dual A_{2A}/A_{2B} AR antagonists containing quinoline or its open-ring bioisosteres based on the structure of triazole-pyrimidine-methylbenzonitrile.

microsomal metabolic stability and *in vivo* pharmacokinetic properties were assessed for optimised compounds.

2. Results and discussion

2.1. Chemistry

The synthetic route of target compounds **7a**–**7l** is shown in Scheme 1. Compound **2** was synthesised from the reaction of 3-bromo-2-methylphenylacetonitrile (**1**) with $(BPin)_2$ catalysed by $Pd(dppf)Cl_2$. Then, compound **3** was acquired from the Suzuki coupling reaction between compound **2** and 4,6-dichloro-2-pyrimidinamine. Subsequently, compound **4** was synthesised via the Sonogashira cross-coupling reaction of compound **3** with trimethylsilylacetylene (TMSA), which further reacted with tetrabutylammonium fluoride (TBAF) in THF to get compound **5**. A copper and sodium L-ascorbate catalysed azide-alkyne coupling between **5** and **6** yielded compounds **7a**–**7b** and **7d**–**7g**. In addition, compound **7b** could be reduced with $SnCl_2$ to obtain compound **7c**. Furthermore, treatment of compound **7d** with LiOH aqueous solution or various amine

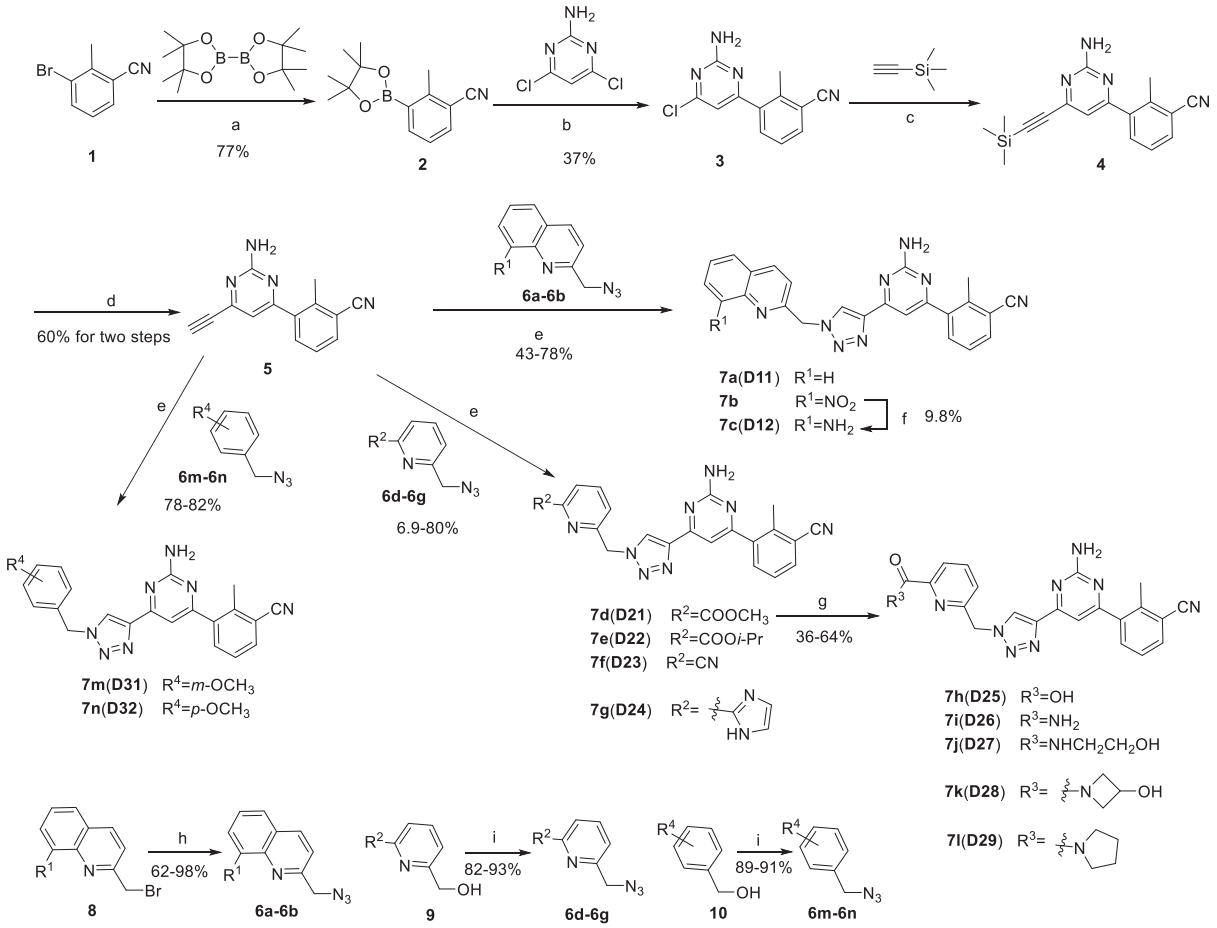

Scheme 1. Synthetic route of target compounds **7a**–**7n**. Reagents and conditions: (a) $Pd(dppf)Cl_2$, $(Bpin)_2$, potassium acetate, 1,4-dioxane, N_2, reflux, 4 h; (b) 4,6-dichloropyrimidin-2-amine, K_2CO_3, $Pd(PPh_3)_4$, DMF, N_2, 45 °C, 5 min, then compound **2** was added, 115 °C, 5 h; (c) Et_3N, TMSA, $Pd(PPh_3)_2Cl_2$, CuI, dry THF, N_2, reflux, 16 h; (d) TBAF(1M in THF), THF, 0 °C to r.t., 20 h; (e) Compound **6**, $CuSO_4{\cdot}5H_2O$, sodium L-ascorbate, 60 °C, DMF, *t*-BuOH, 12 h; (f) $SnCl_2$, 70 °C, 2 h; (g) for **7h**: LiOH, H_2O, *t*-BuOH, r.t., 8 h; for **7i**–**7l**: The corresponding amine derivatives, MeOH, THF, 45 °C, 18 h; (h) TMSiA, DIPEA, THF, r.t., 24 h; (i) DPPA, DBU, THF, r.t., 10 h.

derivatives yielded **7h**–**7l**. The synthesis of intermediates **6** can be achieved by nucleophilic substitution of the corresponding alcohols or bromides with azidotrimethylsilane (TMSiA) or diphenyl azidophosphate (DPPA) with good yields (the synthesis of intermediates **6** can be found in the Supporting information).

To verify the effect of the benzonitrile and quinoline structure on A_2 receptors, compounds **7m**, **7n**, **17**, and **22** were synthesised following the synthetic routes shown in Scheme 1–3. Compounds **7m**–**7n**, which contain a benzene ring instead of the quinoline structure, were synthesised by the azide-alkyne coupling between **5** and **6m**–**6n** in 78–82% yield. The synthesis of compound **17** (Scheme 2) started from 5-methylfuran-2-boronic acid pinacol ester (**11**), according to the synthesis method of compound **7a**, and **17** was generated in moderate yield. In the synthetic route of compound **22**, the intermediate **21** synthesised from compound **18** can be purchased from Sundia Company (the synthesis of intermediate **21** is found in the Supporting information). Intermediate **21** then reacted with TBAF and intermediate **16** in the presence of $CuSO_4{\cdot}5H_2O$ and sodium L-ascorbate to obtain target compound **22** in a one-pot reaction.

2.2. Biology studies

2.2.1. cAMP functional assay

In the hypoxic TME, over-activation of A_2 receptors upregulates cAMP levels by stimulating adenylate cyclase. The abilities of synthesised compounds **7**, **17**, and **22** to inhibit the hA_{2A} or hA_{2B} receptor were studied by evaluating their effect on cAMP production in Chinese hamster ovary (CHO) cells which stably express hA_{2A} AR or hA_{2B} AR[4,9,37].

The cAMP assay results are summarised in Table 1. In the cAMP assay, CHO-K1/ADORA2A/Gα15 cells expressing human A_{2A} AR and CHO-K1/ADORA2b/Gα15 cells expressing human A_{2B} AR were activated by 5′-(N-ethylcarboxamido)adenosine (NECA) and triggered the accumulation of intracellular cAMP concentration. The agonist-induced cAMP intracellular accumulation was inhibited by compounds **7** or ZM241385. The inhibition rates of compounds **7** were determined by comparing the inhibitory activities of the target compounds at a certain concentration with that of ZM241385 at 1 μM. From the cAMP assay results, compounds **7** exhibited good to excellent inhibitory activities on the NECA-triggered cAMP intracellular accumulation in CHO cells expressing human A_{2A} AR (from 43.54% to 107.32%) at 1 μM. It was noted that **7g** and **7i** showed superior inhibition activity to AB928, as a control. At 100 nM, compound **7a** containing quinoline structure showed 16.52% and 3.51% inhibition, respectively, on A_{2A} AR- and A_{2B} AR-mediated cAMP production. It is worth mentioning that the introduction of an amino group as a hydrogen bond donor at C8 of the quinoline moiety was beneficial to the inhibitory activities (Table 1, **7a** versus **7c**), In particular, the inhibition of A_{2B} AR-mediated cAMP production was increased to an impressive 85.43%. Moreover, the replacement of the phenyl ring of the quinoline structure by a ring-opening structure further increased the activity. Compounds **7d**–**7l**, containing the pyridine structure, exhibited better inhibitory

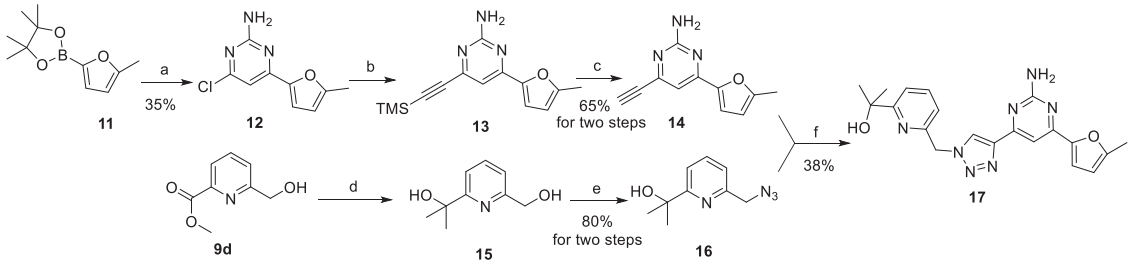

Scheme 2. Synthetic route of the target compound **17**. Reagents and conditions: (a) 4,6-dichloropyrimidin-2-amine, K_2CO_3, $Pd(PPh_3)_4$, DMF, N_2, 45 °C, 5 min, then compound **11** was added, 115 °C, 5 h; (b) Et_3N, TMSA, $Pd(PPh_3)_2Cl_2$, CuI, dry THF, N_2, reflux, 16 h; (c) TBAF(1M in THF), THF, 0 °C to r.t., 20 h; (d) MeMgBr, THF, −10 °C to r.t., 12 h; (e) DPPA, DBU, THF, r.t., 10 h; (f) $CuSO_4{\cdot}5H_2O$, sodium L-ascorbate, 60 °C, DMF, *t*-BuOH, 12 h.

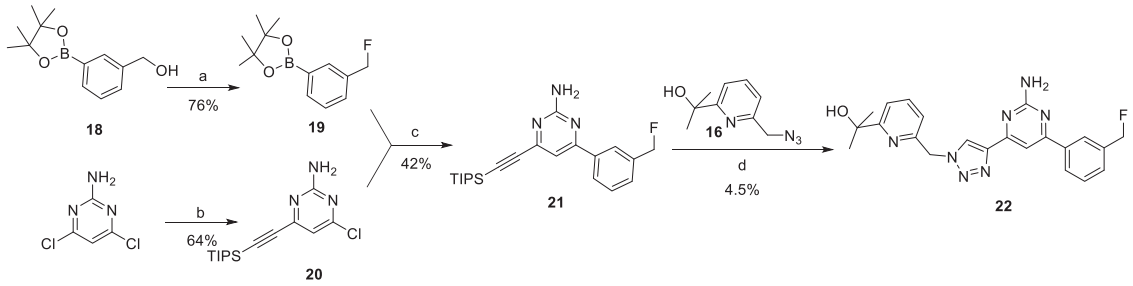

Scheme 3. Synthetic route of the target compound **22**. Reagents and conditions: (a) MsCl, Et_3N, 0 °C, DCM, 1 h, then TBAF (1 M in THF) was added, 50 °C, 12 h; (b) 4,6-dichloropyrimidin-2-amine, TMSA, Et_3N, $Pd(PPh_3)_2Cl_2$, CuI, dry THF, N_2, 80 °C, 12 h; (c) $Pd(dppf)Cl_2$, K_2CO_3, 1,4-dioxane, N_2, 100 °C, 4 h; (d) TBAF (1 M in THF), $CuSO_4{\cdot}5H_2O$, sodium L-ascorbate, H_2O, *t*-BuOH, 60 °C,12 h.

Table 1. Antagonist activity (%inhibition) of compounds **7**, **17**, and **22** at 10–1000 nM on cAMP levels in CHO cells expressing hA_{2A} AR or hA_{2B} AR [a].

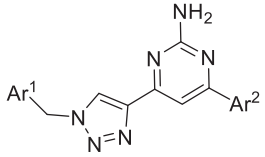

Compound	Ar^1	Ar^2	hA_{2A} AR (%) 1000 nM	hA_{2A} AR (%) 100 nM	hA_{2A} AR (%) 10 nM	hA_{2B} AR (%) 100 nM
7a		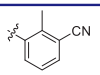	43.54 ± 0.77	16.52 ± 1.90	28.24 ± 8.79	3.51 ± 3.19
7c			48.45 ± 1.45	38.16 ± 10.85	35.9 ± 5.39	85.43 ± 0.04
7d			91.27 ± 4.28	63.38 ± 1.39	40.83 ± 9.01	80.27 ± 1.84
7e			67.76 ± 4.91	50.68 ± 5.51	44.99 ± 1.25	82.45 ± 7.81
7f			92.41 ± 0.43	84.21 ± 2.94	54.91 ± 1.19	102.64 ± 0.24
7g			107.32 ± 0.89	56.02 ± 2.03	19.61 ± 2.13	52.94 ± 3.96
7h			92.61 ± 1.91	55.18 ± 4.27	37.91 ± 2.32	54.75 ± 2.09
7i			102.58 ± 2.82	95.93 ± 3.36	32.73 ± 1.80	103.33 ± 0.63
7j	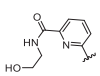		100.79 ± 4.62	82.17 ± 1.26	22.45 ± 6.68	82.38 ± 4.52

(*continued*)

Table 1. Continued.

Compound	Ar^1	Ar^2	hA_{2A} AR (%) 1000 nM	hA_{2A} AR (%) 100 nM	hA_{2A} AR (%) 10 nM	hA_{2B} AR (%) 100 nM
7k	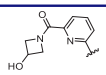	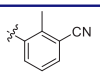	94.87 ± 2.05	70.52 ± 6.37	21.69 ± 5.43	78.28 ± 2.66
7l	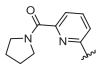		89.66 ± 1.31	52.3 ± 8.46	13.46 ± 3.71	84.34 ± 4.72
7m	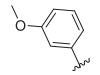		69.63 ± 1.01	28.64 ± 4.03	21.51 ± 4.32	69.38 ± 4.01
7n	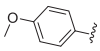		54.77 ± 2.41	29.78 ± 0.38	18.77 ± 3.88	63.52 ± 4.93
17			92.65 ± 2.87	92.28 ± 0.61	17.63 ± 2.78	64.42 ± 0.89
22			93.61 ± 2.76	94.73 ± 4.43	22.39 ± 11.87	19.88 ± 1.85
AB928[b]	AB928	AB928	101.35 ± 5.55	96.8 ± 7.16	20.04 ± 6.46	102.85 ± 1.04

[a]Data are expressed as means ± SEM.
[b]Used as a positive control.

activities against A_{2A} AR than compound **7c** (from 50.68% to 95.93%) at 100 nM, among them, **7f** and **7i** showed 84.21% and 95.93% inhibition, respectively, which were equivalent to that of AB928. Interestingly, at lower concentration (10 nM), they displayed higher inhibition rates than AB928. In addition, the inhibitory activities of **7f** and **7i** on A_{2B} AR-mediated cAMP production were comparable to that of the control compound AB928.

The activities of compounds **7d**–**7l** at 100 nM indicate the substituents at the pyridine structure could influence the inhibitory activities of these compounds on both A_2 ARs. The substituent should be a group that contains a hydrogen bond receptor such as an ester group, cyano group, or amide (**7d**–**7f**, and **7l**). A hydrogen bond donor such as $–NH_2$ and –NH– could also increase the inhibition activities of structures bearing carbonyl group (**7d**–**7e** versus **7i**–**7j**) on both A_{2A} AR and A_{2B} AR. For compounds with an amide moiety, the size of the substituent at the nitrogen atom has a negative influence on the activity (**7i** > **7j** > **7k**). A hydrogen bond donor attached to the carbonyl group was necessary for the inhibitory activities of target compounds on A_{2A} AR, but it has no obvious effect on the inhibitory activities on A_{2B} AR (**7d**–**7e**, and **7l**).

To further validate our design strategy, compounds **7m**–**7n**, containing a benzene ring instead of the pyridine ring or quinoline structure, were synthesised. These compounds exhibited similar inhibitory activity to compounds **7a** and **7c** at concentrations of 1000 nM and 100 nM, but the activities were lower at 10 nM. Moreover, compounds **17** and **22** containing the same Ar^1 fragment as AB928 were synthesised and showed good inhibitory activities at 10 nM, 100 nM, and 1000 nM against A_{2A} AR. However, their activities against A_{2B} AR decreased significantly at 100 nM because of the replacement of the Ar^2 fragment by other structures. The changes in the activities of compounds **7m**–**7n**, **17**, and **22** relative to **7a**, **7c**–**7l**, and AB928 indicated the structures of benzonitrile and pyridine analogues are beneficial to improving the inhibitory activities of target compounds on human A_2 receptor, which was consistent with our design strategy.

We further tested the IC_{50} values of compounds **7f**, **7i**, **17**, **22**, and AB928 in inhibiting the cAMP production of CHO cells expressing hA_{2A} AR or hA_{2B} AR (Table 2). The results indicate the inhibitory activity of compound **7i** on the A_{2A} receptor is similar to that of AB928, and compound **7f** is 4-fold less active than compound **7i**. The inhibitory activities of compounds **17** and **22** were 52-fold and 11-fold less active than compound **7i**, respectively. In addition, the competitive binding experiments of compounds **7f**, **7i**, and AB928 were performed using membrane preparation of HEK-293 cells expressing human A_{2A} AR (Table 3). Their IC_{50} values were 158.0 nM, 63.55 nM, and 25.23 nM, which are consistent with the results of the cAMP assay.

Compound **7i** was also the most effective in inhibiting A_{2B} AR-mediated cAMP production, and the IC_{50} value was 14.12 nM, which is 1.8-fold more active than compound AB928. Compounds without benzonitrile structure (**17** and **22**) had poor inhibitory activities indicating the cyano structure on the benzene ring is closely related to the inhibitory activity of the antagonist on A_{2B} AR.

2.2.2. T Cell activation assay

The effector functions of T cells that express A_2 ARs can be evaluated by measuring specific cytokine production[4,9,38]. In this study, the efficiencies of selected antagonists on IL-2 production (T cell activation) were examined. Two compounds (**7f** and **7i**) were evaluated in this assay and showed sufficient activities to stimulate IL-2 production through T cell activation (Figure 3). The results show the concentration of IL-2 was significantly reduced in the NECA control, which suggests NECA inhibited T cell activation. However, when the antagonist was added, the concentration of IL-2 was restored, indicating the inhibition effect of NECA was blocked. Interestingly, **7i** demonstrated better activity than AB928, suggesting it has potential as an immunotherapy against tumours via T cell activation.

2.2.3. Molecular docking studies

Docking studies were performed at the hA_{2A} and hA_{2B} AR binding sites to simulate the interaction of compound **7i** with these two

Table 2. IC_{50} values of selected compounds on cAMP assays in CHO cells expressing hA_{2A} or hA_{2B} AR[a].

Compound	cAMP IC_{50} (nM)	
	hA_{2A} AR	hA_{2B} AR
7f	24.04 ± 0.06	102.64 ± 0.24%[b], 10.79 ± 0.67%[c]
7i	6.007 ± 0.05	14.12 ± 2.05
17	320.5 ± 94.04	80.03 ± 13.45
22	67.19 ± 10.92	178.5 ± 9.89
AB928	2.754 ± 0.12	25.48 ± 0.35

[a]Data are expressed as means ± SEM.
[b]Percentage of inhibition (I%) determined at 100 nM concentration of compound **7f**.
[c]Percentage of inhibition (I%) determined at 10 nM concentration of compound **7f**.

receptors. The binding modes of compound **7i** at the hA_{2A} AR cavity were analysed by docking simulations using the C-DOCKER protocol of Discovery Studio 2017 R2[39]. The crystal structure of hA_{2A} AR in complex with antagonist ZM241385 (PDB ID: 5IU4) was retrieved from the Protein Data Bank (http://www.rcsb.org/pdb) for the docking calculations. The docking simulation results show that compound **7i** could bind to the active site inside the transmembrane (TM) region and extracellular loops (ECLs) of the human A_{2A} AR similar to the co-crystallized ZM241385[27]. In this binding mode, the phenyl group is located in the proximity of His264, Leu167, Leu267, and Lys153 at the entrance of the hA_{2A} AR cavity (Figure 4(a,c); for more details see supporting information Figure S2). The pyridine and triazole scaffold position in the depth of the binding pocket and both give π–π interaction with the key receptor residue Phe168 (ECL2). This indicates the attachment of an aromatic ring to the triazole facilitates the binding of the inhibitor to the target. In addition, the asparagine residue in TM6 (Asn253) forms H-bond with the N1 atom at the pyridine scaffold and it forms an additional H-bond with the amide group attached to the pyridine ring. The docking results are consistent with the biological results.

The binding mode of hA_{2B} AR was also analysed with the same docking protocols in Discovery Studio 2017 R2. The homology model of hA_{2B} AR was developed using a hA_{2A} AR crystal structure as the template (PDB ID: 6PS7) and has been checked using the Ramachandran plot application within Discovery Studio[40,41]. In the binding mode (Figure 4(b,d); for more details see Supporting information Figure S3), the pyridine scaffold is located at the entrance of the cavity getting close to residue Phe173 in the ECL2 segment, and the methylbenzonitrile moiety is located in the depth of the binding pocket by a π–π interaction with Trp247. In addition, the cyano group has a polar interaction with the amide function of Asn282. The binding mode shows the methylbenzonitrile structure is beneficial to obtaining potent inhibitory activity on A_{2B} AR. Moreover, favourable interactions with the amide group and methyl group are established with the side chains of Ala64 and His280. Thus, the substituents on the pyridine ring may affect the compound affinity.

2.2.4. Microsomal metabolic stability

The metabolic stability is an important focus for further compound optimisation. Compounds **7f**, **7i**, and AB928 were chosen to evaluate the stability in rat liver microsomes and human liver microsomes. For the microsomal metabolic experiment, 7-ethoxycoumarin (7-EC) was used as a control. As shown in Table 4 (see Supporting information for raw data), the $CL_{int(liver)}$ of 7-EC in rats and humans was 10.0 and 9.0 ml/min/g liver, respectively,

Table 3. Radioligand binding affinity data (IC_{50}) for selected compounds against hA_{2A} AR[a].

Compound	cAMP assays IC_{50} (nM)	Radioligand binding assays IC_{50} (nM)
7f	24.04 ± 0.06	158.0 ± 56.42
7i	6.007 ± 0.05	63.55 ± 13.03
AB928	2.754 ± 0.12	25.23 ± 0.74

[a]Data are expressed as means ± SEM.

indicating the experimental test system was reliable. Compounds **7f** and **7i** exhibited good liver microsomes stabilities *in vitro*. They hardly metabolised on human liver microsomes but showed slow metabolism on rat microsomes with $CL_{int(liver)}$ of 0.78 and 1.08 ml/min/g, and both compounds were more stable than AB928 (2.15 ml/min/g in rat liver microsomes).

2.2.5. In vivo pharmacokinetics study

The *in vivo* pharmacokinetic (PK) profiles of compounds **7f** and **7i** were examined in male Balb/c mice (Table 5 and Figure 5). The two compounds showed similar pharmacokinetic properties. After the intravenous (i.v.) administration of 10 mg/kg, the maximum plasma concentration of compounds **7f** and **7i** were 5010.30 μg/l at 0.25 h and 7266.60 μg/l at 0.25 h, respectively. When orally administered at 30 mg/kg, these compounds showed moderate half-lives at a range of 4.12–4.82 h. The absolute bioavailabilities of compounds **7f** and **7i** were 87.7% and 58.8%, respectively. These PK parameters can be used to evaluate the drug-like properties of compounds **7f** and **7i**, so as to clarify their effectiveness and obtain better clinical treatment effects.

3. Conclusion

A series of dual A_{2A}/A_{2B} AR antagonists containing structures of methylbenzonitrile and quinoline or pyridine analogues were designed and synthesised. *In vitro* cAMP assays of target compounds on A_{2A} AR and A_{2B} AR showed good to excellent inhibitory activities. Among these compounds, the inhibitory activity on the A_{2A} receptor of compound **7i** approached that of AB928. Additionally, compound **7i** displayed better inhibitory activity on A_{2B} AR and higher potency in IL-2 production than AB928. Further studies on **7i** demonstrated good liver microsomes stabilities and acceptable *in vivo* PK properties. In future studies, we aim to further improve the potency and drug-like parameters of target compounds. Further optimizations of compound **7i** are still in progress.

4. Experimental section

4.1. General methods for chemistry

All chemicals were purchased from commercial suppliers and used without further purification. Air or moisture sensitive reactions were performed under a positive pressure of nitrogen with oven-dried glassware. Reactions were monitored by thin layer chromatography (TLC), and spots were visualised with iodine vapour or by irradiation with UV light. Flash column chromatography was performed using the Qingdao Haiyang flash silica gel (200–300 mesh). All yields were reported as isolated yields. The melting points were determined on an X-4 binocular microscope melting point apparatus (Beijing Tech Instruments Co., Beijing, China) and were uncorrected. ^{1}H NMR and ^{13}C NMR spectra were recorded on Bruker (^{1}H, 400 MHz or 600 MHz) spectrometers with

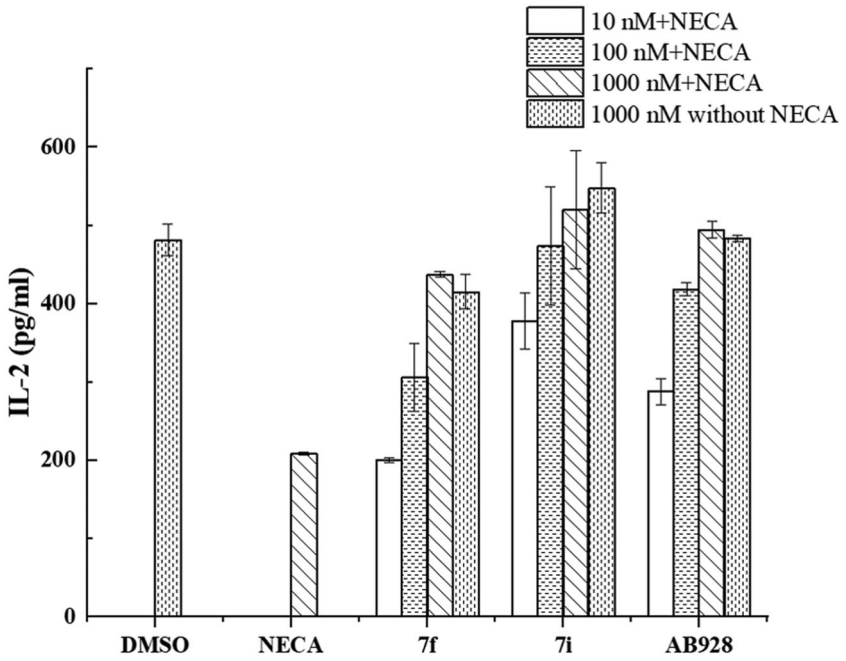

Figure 3. The efficiencies of selected compounds for IL-2 production. The efficiencies of selected antagonists on T-cell activation at 10 nM, 100 nM, and 1000 nM were tested in the presence or absence of 1000 nM NECA. The DMSO control was tested in the absence of both antagonists and NECA. The NECA control was tested without antagonists in the presence of 1000 nM NECA.

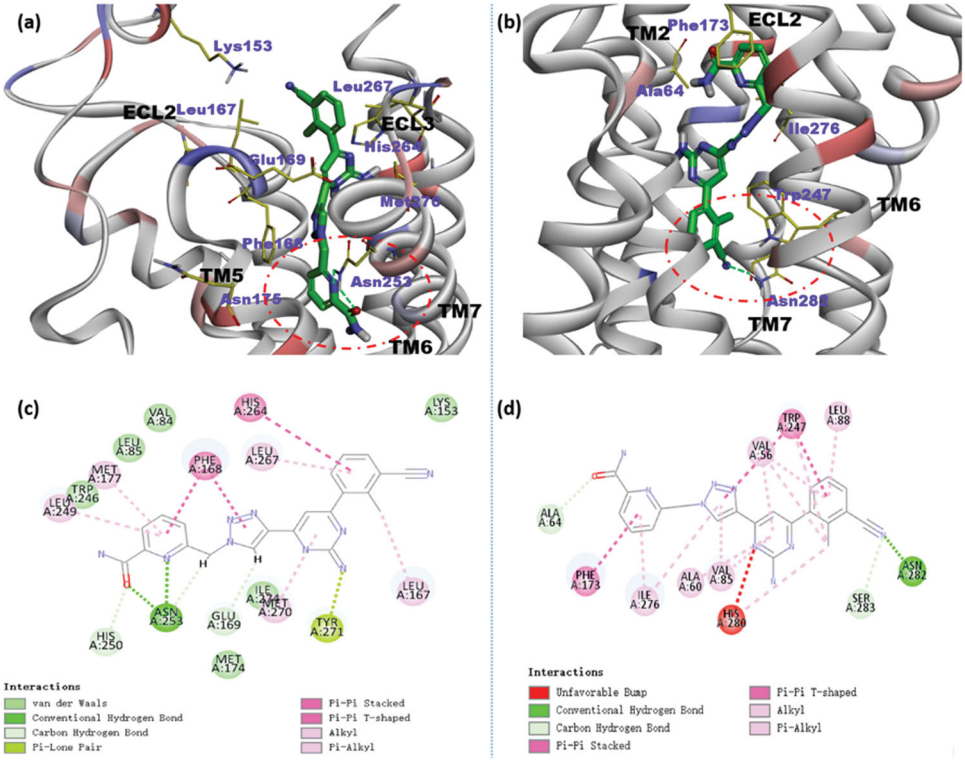

Figure 4. Binding modes of compound **7i** at A_{2A} AR (a) and hA_{2B} AR (b) binding cavities have indicated docking orientations and some key receptor residues. Depths of the two binding pockets have been circled with the red dotted line. 2D diagrams of ligand-target interactions for docking compound **7i** with the A_{2A} AR (c) and hA_{2B} AR (d) predicted by Discovery Studio.

tetramethylsilane as the internal standard. Chemical shifts (δ) are reported in parts per million (ppm) relative to the reference solvents used. The following abbreviations were used to report the multiplicity: br, broad; m, multiplet; s, singlet; d, doublet; t, triplet; q, quartette; dd, doublet of doublets; dt, doublet of triplets. High-resolution mass spectrometry results were recorded on the Thermo Q-Exactive time-of-flight LC/MS system.

4.1.1. Synthesis of 2-methyl-3-(4,4,5,5-tetramethyl-1,3,2-dioxaborolan-2-yl)benzonitrile (2)

To a solution of 3-bromo-2-methylbenzonitrile (10.00 g, 51 mmol) in 1,4-dioxane (100 ml), Bis(pinacolato)diboron (15.54 g, 61 mmol), potassium acetate (10.01 g, 102 mmol) and $Pd(dppf)Cl_2$ (1.12 g, 1.53 mmol) were added under nitrogen. The reaction was refluxed for 5 h and was cooled down to room

Table 4. Metabolic stability assay in rat and human liver microsomes[a].

	Microsomal metabolic stability					
	$T_{1/2}$ (min)		$CL_{int(liver)}$(mL/min/g)		Remaining (%, $T = 60$min)	
Compound	Hum	Rat	Hum	Rat	Hum	Rat
7f	n.c.	93.65	n.c.	0.78	104.65	64.04
7i	1155	67.28	0.06	1.08	98.76	50.67
AB928	433.13	33.8	0.17	2.15	94.40	28.10
7-EC	8.12	7.26	9.0	10.0	0.72	0.35

[a]$T_{1/2}$, half-life, $CL_{int(liver)}$, intrinsic clearance, n.c., not calculated.

temperature. The precipitate formed in the mixture was filtered. 50 ml of water was added to the filtrate and then extracted with ethyl acetate (30 ml × 3). The combined organic layers were washed with brine and dried over Na_2SO_4. After filtration and evaporation, the condensation was purified with a silica gel column (petroleum ether/ethyl acetate = 20:1) to yield compound **2** as white solid (11.15 g, 77%). ^{1}H NMR (600 MHz, DMSO-d_6) δ (ppm) 7.91 (d, $J = 7.2$ Hz, 1H), 7.86 (t, $J = 6.7$ Hz, 1H), 7.38 (q, $J = 6.9$ Hz, 1H), 2.66 (s, 3H), 1.31 (s, 12H). MS (ESI), *m/z*: 244.23 $[M + H]^+$.

4.1.2. Synthesis of 3-(2-amino-6-chloropyrimidin-4-yl)-2-methylbenzonitrile (3)

4,6-Dichloropyrimidin-2-amine (4.55 g, 27.77 mmol), K_2CO_3 (7.68 g, 55.53 mmol) and $Pd(PPh_3)_4$ (1.07 g, 0.93 mmol) were dissolved in DMF (50 ml) under nitrogen. Then, water (5 ml) was added and the mixture was heated to 45 °C. A solution of compound **2** (4.50 g, 18.51 mmol) in DMF was added dropwise to the reaction mixture. The mixture was then heated and stirred at 115 °C for 5 h and was cooled down to room temperature. 50 ml of water was added and the mixture solution was extracted three times with ethyl acetate (30 ml × 3). The combined organic layers were washed with brine, dried over Na_2SO_4, and concentrated. The condensation was purified with a silica gel column (petroleum ether/ethyl acetate = 10:1) to yield compound **3** as white solid (1.68 g, 37%).^{1}H NMR (600 MHz, DMSO-d_6) δ (ppm) 7.89 (d, $J = 7.7$ Hz, 1H), 7.70 (d, $J = 7.2$ Hz, 1H), 7.50 (t, $J = 7.7$ Hz, 1H), 7.29 (s, 2H), 6.86 (s, 1H), 2.51 (s, 3H). MS (ESI), *m/z*: 245.15 $[M + H]^+$.

4.1.3. Synthesis of 3-(2-amino-6-((trimethylsilyl)ethynyl)pyrimidin-4-yl)-2-methylbenzonitrile (4)

To a solution of compound **3** (1.00 g, 4.08 mmol) in dry THF (40 ml) were added triethylamine (TEA) (1.24 g, 12.24 mmol) and trimethylsilylacetylene (0.601 g, 6.12 mmol), and the reaction mixture was stirred under a nitrogen atmosphere. After stirring for 5 min, $Pd(PPh_3)_2Cl_2$ (72 mg, 0.102 mmol) and CuI (39 mg, 0.204 mmol) were added. The reaction mixture was refluxed overnight before being cooled to room temperature. The mixture was evaporated under reduced pressure and dissolved in ethyl acetate (30 ml). The mixture was stirred for 5 min, Suction filtration to remove insoluble matter. Then the organic layer was washed with brine, dried over anhydrous Na_2SO_4, and concentrated under reduced pressure. The resulting compound **4** as black solid (1.12 g) was used in the next step without further purification. ^{1}H NMR (600 MHz, DMSO-d_6) δ (ppm) 7.63 (dd, $J = 7.7$, 1.2 Hz, 1H), 7.45 (dd, $J = 7.7$, 1.2 Hz, 1H), 7.24 (t, $J = 7.8$ Hz, 1H), 6.74 (s, 2H), 6.56 (s, 1H), 2.25 (s, 3H), 0.00 (s, 9H). MS (ESI), *m/z*: 307.40 $[M + H]^+$.

Table 5. Pharmacokinetic parameters of compounds **7f** and **7i** [a].

	7f		7i	
Parameter	Oral	i.v.	Oral	i.v.
$t_{1/2}$ (h)	4.12	2.67	4.82	2.19
t_{max}(h)	2.00	0.25	1.00	0.08
C_{max}(μg/L)	7162.80	5010.30	1007.40	7266.60
$C_{max/Dose}$ [b]	238.76	501.03	33.58	726.66
$AUC_{0\to t}$(μg/L*h)	45,490.39	1728.68	7904.90	4484.58
$AUC_{0\to t/Dose}$ [c]	1516.35	1728.68	263.50	448.46
$AUC_{0\to\infty}$(μg/L*h)	46,232.45	17315.97	8145.18	4484.81
$AUC_{0\to\infty/Dose}$ [c]	1541.08	1731.60	271.51	448.48
F(%)	87.7		58.8	

[a]PK parameters (mean, $n = 3$), C_{max}, maximum concentration; T_{max}, time to reach C_{max}; $AUC_{0\to t}$, Area under the curve from zero to the last measurable plasma concentration; $AUC_{0\to\infty}$, Area under the curve from the last measurable plasma concentration to infinity.
[b]Unit is (μg/L)/(mg/kg).
[c]Unit is (μg/L*h)/(mg/kg).

4.1.4. Synthesis of 3-(2-amino-6-ethynylpyrimidin-4-yl)-2-methylbenzonitrile (5)

Compound **4** (1.12 g) was dissolved in dry THF (15 ml) under a nitrogen atmosphere. And 6 ml of TBAF (1 M in THF) was added to the mixture dropwise under external ice bath cooling, and the reaction was stirred at room temperature for 20 h. The reaction mixture was quenched by pouring into aqueous NH_4Cl (30 ml) at 0 °C and extracted with ethyl acetate (30 ml × 3). The combined organic layer was washed with water (30 ml), dried on $MgSO_4$, evaporated under reduced pressure and purified by column chromatography (petroleum ether/ethyl acetate = 3:1) to obtain pure compound **5** as brown solid (0.575 g, 60% for two steps). ^{1}H NMR (600 MHz, DMSO-d_6) δ (ppm) 7.89 (dd, $J = 7.7$, 1.4 Hz, 1H), 7.70 (dd, $J = 7.8$, 1.4 Hz, 1H), 7.49 (t, $J = 7.8$ Hz, 1H), 7.00 (s, 2H), 6.86 (s, 1H), 4.52 (s, 1H), 2.51 (s, 3H). MS (ESI), *m/z*: 235.41 $[M + H]^+$.

4.1.5. General synthetic procedure for compounds 7a, 7d–7g, 7m–7n

To a solution of compound **5** (350 mg, 1.50 mmol) in DMF (3 ml), *t*-BuOH (15 ml) and water (9 ml) were added compound **6** (1.65 mmol), $CuSO_4{\cdot}5H_2O$ (11 mg, 0.045 mmol) and sodium L-ascorbate (13 mg, 0.068 mmol). The reaction was allowed to be stirred for 12 h at 65 °C and then concentrated under reduced pressure to remove the solvent. The concentrate was then purified by column chromatography (DCM/MeOH =50:1 to 25:1) to afford compounds **7a**, **7d**–**7g**, **7m**–**7n**.

3-(2-Amino-6–(1-(quinolin-2-ylmethyl)-1*H*-1,2,3-triazol-4-yl)pyrimidin-4-yl)-2-methylbenzonitrile (**7a**), tawny solid. Yield 78%; m.p. 203–204 °C; ^{1}H NMR (600 MHz, DMSO-d_6) δ (ppm) 8.78 (s, 1H), 8.43 (d, $J = 8.5$ Hz, 1H), 8.01 (d, $J = 8.1$ Hz, 1H), 7.97 (d, $J = 8.5$ Hz, 1H), 7.90 (d, $J = 7.7$ Hz, 1H), 7.81–7.74 (m, 2H), 7.63 (t, $J = 7.5$ Hz, 1H), 7.52 (t, $J = 7.7$ Hz, 1H), 7.47 (d, $J = 8.5$ Hz, 1H), 7.30 (s, 1H), 6.89 (s, 2H), 6.06 (s, 2H), 2.56 (s, 3H). ^{13}C NMR (151 MHz, DMSO-d_6) δ (ppm) 166.12, 163.00, 161.69, 157.57, 154.72, 146.37, 145.34, 139.44, 138.47, 136.97, 133.00, 132.66, 129.55, 128.02, 127.38, 126.53, 126.36, 126.31, 125.10, 117.40, 112.62, 104.47, 54.52, 17.67. HRMS (ESI) calcd for $C_{24}H_{19}N_8$ $[M + H]^+$: 419.17272, found: 419.17477.

Methyl 6-((4-(2-amino-6-(3-cyano-2-methylphenyl)pyrimidin-4-yl)-1*H*-1,2,3-triazol-1-yl)methyl)picolinate (**7d**), tawny solid. Yield 78%; m. p. 105–106 °C; ^{1}H NMR (600 MHz, DMSO-d_6) δ (ppm) 8.72 (s, 1H), 8.07–8.02 (m, 2H), 7.89 (dd, $J = 7.7$, 1.2 Hz, 1H), 7.75 (dd, $J = 7.8$, 1.2 Hz, 1H), 7.55–7.50 (m, 2H), 7.27 (s, 1H), 6.89 (s, 2H), 5.92 (s, 2H), 3.88 (s, 3H), 2.55 (s, 3H). ^{13}C NMR (151 MHz, DMSO-d_6) δ (ppm) 167.16, 165.28, 164.08, 158.60, 155.83, 147.81, 146.45,

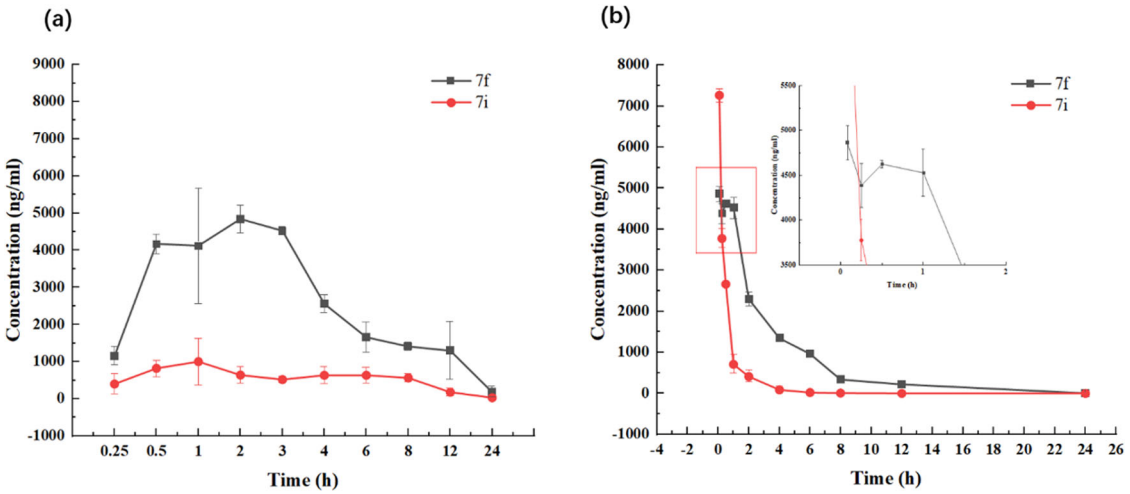

Figure 5. Plasma concentration-time profiles of compounds **7f** and **7i** following oral administration (a) and intravenous administration (b).

140.46, 139.56, 139.50, 134.09, 133.74, 127.43, 126.28, 125.92, 124.80, 118.47, 113.67, 105.48, 54.86, 53.01, 18.72. HRMS (ESI) calcd for $C_{22}H_{19}N_8O_2$ $[M+H]^+$: 427.16255, found: 427.16251.

Isopropyl 6-((4-(2-amino-6-(3-cyano-2-methylphenyl)pyrimidin-4-yl)-1*H*-1,2,3-triazol-1-yl)methyl)picolinate (**7e**), white solid. Yield 80%; m.p. 128–129 °C; ^{1}H NMR (600 MHz, DMSO-d_6) δ (ppm) 8.73 (s, 1H), 8.05–7.98 (m, 2H), 7.90 (dd, J = 7.8, 1.4 Hz, 1H), 7.75 (dd, J = 7.7, 1.4 Hz, 1H), 7.52 (td, J = 7.8, 0.7 Hz, 1H), 7.48 (dd, J = 7.5, 1.4 Hz, 1H), 7.27 (s, 1H), 6.88 (s, 2H), 5.93 (s, 2H), 5.15 (hept, J = 6.3 Hz, 1H), 2.55 (s, 3H), 1.32 (d, J = 6.3 Hz, 6H). ^{13}C NMR (151 MHz, DMSO-d_6) δ (ppm) 166.07, 163.13, 163.01, 157.55, 154.76, 147.18, 145.38, 139.39, 138.47, 138.33, 133.00, 132.66, 126.36, 124.99, 124.77, 123.54, 117.39, 112.59, 104.40, 68.39, 53.75, 20.96, 17.64. HRMS (ESI) calcd for $C_{24}H_{23}N_8O_2$ $[M+H]^+$: 455.19385, found: 455.19458.

6-((4-(2-Amino-6-(3-cyano-2-methylphenyl)pyrimidin-4-yl)-1*H*-1,2,3-triazol-1-yl)methyl)picolinonitrile (**7f**), off white solid. Yield 41%; m.p. 147–148 °C; ^{1}H NMR (600 MHz, DMSO-d_6) δ (ppm) 8.74 (s, 1H), 8.12 (t, J = 7.8 Hz, 1H), 8.03 (d, J = 7.7 Hz, 1H), 7.90 (d, J = 7.7 Hz, 1H), 7.76 (d, J = 7.7 Hz, 1H), 7.70 (d, J = 8.0 Hz, 1H), 7.52 (t, J = 7.7 Hz, 1H), 7.28 (s, 1H), 6.89 (s, 2H), 5.94 (s, 2H), 2.55 (s, 3H). ^{13}C NMR (151 MHz, DMSO-d_6) δ (ppm) 167.18, 164.08, 158.57, 157.30, 146.45, 140.45, 139.86, 139.56, 134.09, 133.74, 132.72, 129.02, 127.43, 126.96, 126.17, 118.47, 117.67, 113.67, 105.50, 54.30, 18.72. HRMS (ESI) calcd for $C_{21}H_{16}N_9$ $[M+H]^+$: 394.15232, found: 394.15234.

3-(6-(1-((6-(1*H*-imidazol-2-yl)pyridin-2-yl)methyl)-1*H*-1,2,3-triazol-4-yl)-2-aminopyrimidin-4-yl)-2-methylbenzonitrile (**7 g**), grey solid. Yield 6.9%; m.p. 139–140 °C; ^{1}H NMR (600 MHz, DMSO-d_6) δ (ppm) 12.67 (s, 1H), 8.79 (s, 1H), 7.99 (d, J = 7.9 Hz, 1H), 7.92–7.88 (m, 2H), 7.75 (dd, J = 7.8, 1.4 Hz, 1H), 7.52 (t, J = 7.7 Hz, 1H), 7.28 (s, 2H), 7.20 (d, J = 7.6 Hz, 1H), 7.09 (s, 1H), 6.85 (s, 2H), 5.85 (s, 2H), 2.55 (s, 3H). ^{13}C NMR (151 MHz, DMSO-d_6) δ (ppm) 167.10, 164.07, 158.68, 154.85, 149.37, 146.51, 145.44, 140.45, 139.55, 139.04, 134.09, 133.74, 130.18, 127.43, 125.72, 121.67, 119.49, 119.37, 118.46, 113.67, 105.63, 55.29, 18.72. HRMS (ESI) calcd for $C_{23}H_{19}N_{10}$ $[M+H]^+$: 435.17887, found: 435.17847.

3-(2-Amino-6-(1-(3-methoxybenzyl)-1*H*-1,2,3-triazol-4-yl)pyrimidin-4-yl)-2-methylbenzonitrile (**7 m**), grey solid. Yield 82%; m.p. 163–164 °C; ^{1}H NMR (400 MHz, DMSO-d_6) δ (ppm) 8.61(s, 1H), 7.84 (d, J = 7.7 Hz, 1H), 7.70 (d, J = 7.7 Hz, 1H), 7.47 (t, J = 7.7 Hz, 1H), 7.27 (t, J = 7.9 Hz, 1H), 7.21(s, 1H), 6.96–6.93 (m, 1H), 6.88 (dd, J = 7.7, 1.5 Hz, 2H), 6.83 (s, 2H), 5.63 (s, 2H), 3.71 (s, 3H), 2.50 (s, 3H). ^{13}C NMR (101 MHz, DMSO-d_6) δ (ppm) 167.19, 164.14, 160.02, 158.68, 146.52, 140.52, 139.62, 137.71, 134.15, 133.79, 130.55, 127.48, 125.20, 120.72, 118.53, 114.47, 114.15, 113.74, 105.55, 55.68, 53.55, 18.78. HRMS (ESI) calcd for $C_{22}H_{20}N_7O$ $[M+H]^+$: 398.17238, found: 398.17227.

3-(2-Amino-6-(1-(4-methoxybenzyl)-1*H*-1,2,3-triazol-4-yl)pyrimidin-4-yl)-2-methylbenzonitrile (**7n**), white solid. Yield 78%; m.p. 149–150 °C; ^{1}H NMR (400 MHz, DMSO-d_6) δ (ppm) 8.54 (s, 1H), 7.84 (d, J = 7.7 Hz, 1H), 7.70 (dd, J = 7.7, 1.0 Hz, 1H), 7.46 (t, J = 7.7 Hz, 1H), 7.36–7.30 (m, 2H), 7.21 (s, 1H), 6.91 (m, 2H), 6.83 (s, 2H), 5.58 (s, 2H), 3.70 (s, 3H), 2.50 (s, 3H). ^{13}C NMR (101 MHz, DMSO-d_6) δ (ppm) 167.17, 164.14, 159.78, 158.71, 146.49, 140.52, 139.61, 134.14, 133.77, 130.35, 128.16, 127.46, 124.82, 118.53, 114.74, 113.74, 105.51, 55.69, 53.19, 18.77. HRMS (ESI) calcd for $C_{22}H_{20}N_7O$ $[M+H]^+$: 398.17238, found: 398.17218.

4.1.6. Synthesis of 3-(2-amino-6-(1-((8-aminoquinolin-2-yl)methyl)-1H-1,2,3-triazol-4-yl)pyrimidin-4-yl)-2-methylbenzonitrile (7c)

3-(2-Amino-6-(1-((8-nitroquinolin-2-yl)methyl)-1*H*-1,2,3-triazol-4-yl)pyrimidin-4-yl)-2-methylbenzonitrile (**7b**) was prepared in the same way as compound **7a** from compound **5** and 2-(azidomethyl)-8-nitroquinoline (**6b**), yellow solid. Yield 43%; MS (ESI), *m/z*: 464.31 $[M+H]^+$.

Compound **7b** (100 mg, 0.216 mmol) was dissolved in ethanol (15 ml) at room temperature, then $SnCl_2$ (205 mg, 1.08 mmol) was added and the mixture was stirred at 70 °C for 2 h. After the completion of the reaction, the mixture was poured into water (50 ml) and concentrated under reduced pressure. The crude residue was purified by reverse silica gel column chromatography (MeOH/H_2O = 0% to 50%) and recrystallized from methanol to afford the compound **7c**, off white solid. Yield 9.8%; m.p. 268–269 °C; ^{1}H NMR (600 MHz, DMSO-d_6) δ (ppm) 8.79 (s, 1H), 8.23 (d, J = 8.5 Hz, 1H), 7.89 (dd, J = 7.7, 1.2 Hz, 1H), 7.76 (dd, J = 7.8, 1.1 Hz, 1H), 7.52 (t, J = 7.7 Hz, 1H), 7.42 (d, J = 8.5 Hz, 1H), 7.32–7.27 (m, 2H), 7.07 (dd, J = 8.1, 1.1 Hz, 1H), 6.90–6.83 (m, 3H), 5.99 (s, 2H), 5.81 (s, 2H), 2.55 (s, 3H). ^{13}C NMR (151 MHz, DMSO-d_6) δ (ppm) 167.11, 164.10, 158.71, 152.06, 146.38, 145.21, 140.46, 139.57, 137.82, 136.84, 134.11, 133.73, 128.43, 128.17, 127.42, 126.03, 120.37, 118.48, 114.06, 113.67, 109.65, 105.55, 55.60, 18.73. HRMS (ESI) calcd for $C_{24}H_{20}N_9$ $[M+H]^+$: 434.18362, found: 434.18289.

4.1.7. Synthesis of 6-((4-(2-amino-6–(3-cyano-2-methylphenyl)pyrimidin-4-yl)-1H-1,2,3-triazol-1-yl)methyl)picolinic acid (7h)

Compound **7d** (128 mg, 0.30 mmol) were dissolved in a mixed solution of *tert* butanol (10 ml) and water (5 ml). Then LiOH (18.5 mg, 0.441 mmol) was added and the reaction mixture was continue stirred for 8 h. After reaction, aqueous HCl (1 M) was added to adjust the pH to 5–6. Next, the mixture solution was extracted with ethyl acetate (20 ml × 3). The combined organic layer was washed with brine (30 ml), dried over Na_2SO_4, then evaporation. The condensation was purified with a silica gel column (DCM/MeOH= 20: 1) to yield compound **7h**, white solid. Yield 65%; m.p. 176–177 °C; ^{1}H NMR (600 MHz, DMSO-d_6) δ (ppm) 13.32 (s, 1H), 8.72 (s, 1H), 8.01 (d, J = 6.3 Hz, 2H), 7.89 (dd, J = 7.8, 1.3 Hz, 1H), 7.76 (dd, J = 7.8, 1.3 Hz, 1H), 7.52 (t, J = 7.7 Hz, 2H), 7.27 (s, 1H), 6.89 (s, 2H), 5.91 (s, 2H), 2.55 (s, 3H). ^{13}C NMR (151 MHz, DMSO-d_6) δ (ppm) 167.15, 166.31, 164.09, 158.63, 155.48, 146.44, 140.46, 139.56, 139.30, 134.09, 133.73, 127.43, 125.89, 125.84, 124.59, 118.47, 113.67, 105.49, 55.38, 18.72. HRMS (ESI) calcd for $C_{21}H_{15}N_8O_2$ [M-H]$^-$: 411.13235, found: 411.13293.

4.1.8. General synthetic procedure for compounds 7i–7l

A solution of compound **7d** (50 mg, 0.12 mmol) in MeOH (3 ml) and THF (3 ml) was cooled to −10 °C and ammonia or its derivatives (2.4 mmol) was added under nitrogen. The reaction mixture was stirred at 45 °C for 4–16 h. The reaction progress was monitored by TLC. After completion of the reaction, the reaction mixture was diluted with water (15 ml) and extracted with ethyl acetate (10 ml × 3). The combined organic phase was washed with brine (20 ml), dried over anhydrous Na_2SO_4, filtered, and concentrated under reduced pressure. The reaction residue thus obtained was purified by flash column chromatography (DCM/MeOH = 50:1 to 20:1) to afford the target compounds **7i-7l**.

6-((4-(2-Amino-6-(3-cyano-2-methylphenyl)pyrimidin-4-yl)-1*H*-1,2,3-triazol-1-yl)methyl)picolinamide (**7i**), white solid. Yield 44%; m.p. 151–152 °C; ^{1}H NMR (600 MHz, DMSO-d_6) δ (ppm) 8.83 (s, 1H), 8.03 (t, J = 7.7 Hz, 1H), 7.99 (dd, J = 7.7, 1.2 Hz, 1H), 7.94 (s, 1H), 7.89 (dd, J = 7.7, 1.2 Hz, 1H), 7.76 (dd, J = 7.8, 1.1 Hz, 1H), 7.73 (s, 1H), 7.52 (t, J = 7.7 Hz, 2H), 7.27 (s, 1H), 6.86 (s, 2H), 5.89 (s, 2H), 2.55 (s, 3H). ^{13}C NMR (151 MHz, DMSO-d_6) δ (ppm) 167.11, 165.89, 164.08, 158.67, 154.30, 150.49, 146.46, 140.45, 139.57, 139.56, 134.10, 133.74, 127.43, 126.01, 125.31, 121.71, 118.47, 113.67, 105.61, 54.83, 18.72. HRMS (ESI) calcd for $C_{21}H_{18}N_9O$ [M + H]$^+$: 412.16288, found: 412.16293.

6-((4-(2-Amino-6-(3-cyano-2-methylphenyl)pyrimidin-4-yl)-1*H*-1,2,3-triazol-1-yl)methyl)-N-(2-hydroxyethyl)picolinamide (**7j**), white solid. Yield 64%; m.p. 208–209 °C; ^{1}H NMR (600 MHz, DMSO-d_6) δ (ppm) 8.80 (s, 1H), 8.55 (t, J = 5.9 Hz, 1H), 8.05–7.99 (m, 2H), 7.90 (dd, J = 7.7, 1.3 Hz, 1H), 7.76 (dd, J = 7.7, 1.3 Hz, 1H), 7.52 (t, J = 7.7 Hz, 1H), 7.45 (dd, J = 7.4, 1.4 Hz, 1H), 7.28 (s, 1H), 6.87 (s, 2H), 5.91 (s, 2H), 4.80 (t, J = 5.4 Hz, 1H), 3.52 (q, J = 5.8 Hz, 2H), 3.39 (q, J = 6.0 Hz, 2H), 2.55 (s, 3H). ^{13}C NMR (151 MHz, DMSO-d_6) δ (ppm) 167.13, 164.07, 163.76, 158.62, 154.42, 150.18, 146.55, 140.45, 139.74, 139.56, 134.09, 133.73, 127.42, 125.93, 125.21, 121.70, 118.46, 113.67, 105.59, 60.11, 54.93, 42.08, 18.72. HRMS (ESI) calcd for $C_{23}H_{22}N_9O_2$ [M + H]$^+$: 456.18910, found: 456.18927.

3-(2-Amino-6-(1-((6–(3-hydroxyazetidine-1-carbonyl)pyridin-2-yl)methyl)-1*H*-1,2,3-triazol-4-yl)pyrimidin-4-yl)-2-methylbenzonitrile (**7k**), grey solid. Yield 36%; m.p. 243–244 °C; ^{1}H NMR (600 MHz, DMSO-d_6) δ (ppm) 8.71 (s, 1H), 8.01 (t, J = 7.8 Hz, 1H), 7.90 (ddd, J = 7.8, 4.8, 1.2 Hz, 2H), 7.76 (dd, J = 7.8, 1.4 Hz, 1H), 7.57 (dd, J = 7.8, 1.0 Hz, 1H), 7.52 (td, J = 7.7, 0.7 Hz, 1H), 7.27 (s, 1H), 6.86 (s, 2H), 5.91 (s, 2H), 5.64 (d, J = 6.3 Hz, 1H), 4.43 (ddd, J = 10.7, 6.7, 1.5 Hz, 1H), 4.41 − 4.36 (m, 1H), 4.20 (ddd, J = 10.9, 6.8, 1.7 Hz, 1H), 4.00 (ddd, J = 10.4, 4.1, 1.4 Hz, 1H), 3.73 (ddd, J = 10.7, 4.3, 1.3 Hz, 1H), 2.55 (s, 3H). ^{13}C NMR (151 MHz, DMSO-d_6) δ (ppm) 167.11, 164.20, 164.08, 158.67, 154.14, 151.77, 146.38, 140.49, 139.58, 139.06, 134.10, 133.72, 127.41, 126.18, 124.56, 122.99, 118.48, 113.66, 105.57, 64.45, 61.32, 59.07, 54.49, 18.71. HRMS (ESI) calcd for $C_{24}H_{22}N_9O_2$ [M + H]$^+$: 468.18910, found: 468.18942.

3-(2-Amino-6-(1-((6–(2-(hydroxymethyl)pyrrolidine-1-carbonyl)-pyridin-2-yl)methyl)-1*H*-1,2,3-triazol-4-yl)pyrimidin-4-yl)-2-methylbenzonitrile (**7l**), white solid. Yield 52%; m.p. 98–99 °C; ^{1}H NMR (600 MHz, DMSO-d_6) δ (ppm) 8.72 (s, 1H), 7.98 (t, J = 7.8 Hz, 1H), 7.89 (d, J = 7.7 Hz, 1H), 7.75 (d, J = 6.9 Hz, 1H), 7.71 (d, J = 7.6 Hz, 1H), 7.52 (t, J = 7.0 Hz, 2H), 7.28 (s, 1H), 6.88 (s, 2H), 5.91 (s, 2H), 3.44 (t, J = 7.0 Hz, 2H), 3.32 (t, J = 6.8 Hz, 2H), 2.55 (s, 3H), 1.75 (p, J = 6.8 Hz, 2H), 1.66 (p, J = 6.8 Hz, 2H). ^{13}C NMR (151 MHz, DMSO-d_6) δ (ppm) 167.11, 165.13, 164.09, 158.67, 154.22, 153.77, 146.31, 140.46, 139.52, 138.88, 134.05, 133.73, 127.43, 126.38, 123.69, 123.30, 118.46, 113.67, 105.41, 54.53, 48.78, 46.95, 26.46, 23.86, 18.69. HRMS (ESI) calcd for $C_{25}H_{24}N_9O$ [M + H]$^+$: 466.20983, found: 466.20834.

4.1.9. Synthesis of 2-(6-((4-(2-amino-6-(5-methylfuran-2-yl)pyrimidin-4-yl)-1H-1,2,3-triazol-1-yl)methyl)pyridin-2-yl)propan-2-ol (17)

Compound **17** was prepared in the same way as **7a** from 4-ethynyl-6-(5-methylfuran-2-yl)pyrimidin-2-amine (**14**) with 2-(6-(azidomethyl)pyridin-2-yl)propan-2-ol (**16**).

2-(6-((4-(2-Amino-6-(5-methylfuran-2-yl)pyrimidin-4-yl)-1*H*-1,2,3-triazol-1-yl)methyl)pyridin-2-yl)propan-2-ol (**17**), pale yellow solid. Yield 38%; m.p. 188–189 °C; ^{1}H NMR (600 MHz, DMSO-d_6) δ 8.61 (s, 1H), 7.80 (t, J = 7.8 Hz, 1H), 7.61 (d, J = 7.6 Hz, 1H), 7.46 (s, 1H), 7.14 (d, J = 3.3 Hz, 1H), 7.10 (d, J = 7.5 Hz, 1H), 6.70 (s, 2H), 6.33 (dd, J = 3.3, 1.0 Hz, 1H), 5.80 (s, 2H), 5.21 (s, 1H), 2.40 (s, 3H), 1.38 (s, 6H). ^{13}C NMR (151 MHz, DMSO) δ 168.59, 164.25, 158.60, 156.78, 155.20, 153.56, 150.73, 146.48, 138.22, 125.52, 119.87, 118.43, 113.31, 109.37, 99.17, 72.73, 55.08, 31.03, 14.05. HRMS (ESI) calcd for $C_{20}H_{22}N_7O_2$ [M + H]$^+$: 392.18295, found: 392.18250.

4.1.10. Synthesis of 2-(6-((4-(2-amino-6-(3-(fluoromethyl)phenyl)-pyrimidin-4-yl)-1H-1,2,3-triazol-1-yl)methyl)pyridin-2-yl)propan-2-ol (22)

To a solution of compound **21** (384 mg, 1.00 mmol) and compound **16** (288 mg, 1.50 mmol) in *t*-BuOH (4 ml) and water (4 ml) were added $CuSO_4{\cdot}5H_2O$ (25 mg, 0.10 mmol), sodium L-ascorbate (40 mg, 0.20 mmol) and TBAF (1 M in THF) (2.00 ml, 2.00 mmol). The reaction was allowed to be stirred for 12 h at 60 °C and then concentrated under reduced pressure to remove the solvent. The concentrate was then purified by column chromatography (DCM/MeOH = 50:1) to afford compound **22**, white solid. Yield 4.5%; m.p. 76–77 °C; ^{1}H NMR (600 MHz, DMSO-d_6) δ 8.68 (s, 1H), 8.21 (s, 1H), 8.17–8.13 (m, 1H), 7.80 (t, J = 7.8 Hz, 1H), 7.74 (s, 1H), 7.61 (d, J = 8.0 Hz, 1H), 7.58 (m, 2H), 7.12 (d, J = 7.6 Hz, 1H), 6.81 (s, 2H), 5.82 (s, 2H), 5.54 (d, J = 47.6 Hz, 2H), 5.22 (s, 1H), 1.38 (s, 6H). ^{13}C NMR (151 MHz, DMSO) δ 167.53, 163.62, 163.41, 158.05, 152.49, 145.44, 137.16, 136.20 (d, J = 16.7 Hz), 130.87 (d, J = 9.5 Hz), 129.17 (d, J = 5.8 Hz), 128.14 (d, J = 11.8 Hz), 126.43 (d, J = 2.8 Hz), 125.42 (d, J = 5.9 Hz), 124.70, 118.79, 117.37, 100.42, 83.47 (d, J = 162.3 Hz), 71.66, 54.03, 29.96. HRMS (ESI) calcd for $C_{22}H_{23}FN_7O$ [M + H]$^+$: 420.19426, found: 420.19394.

4.2. Pharmacology

4.2.1. Cyclic AMP functional assay

CHO-K1/ADORA2A/Gα15 cells expressing human A_{2A} AR and CHO-K1/ADORA2b/Gα15 cells expressing human A_{2B} AR were both constructed by Genscript Biotech Corporation. These two types of cells were cultured in an F12K complete medium (Gibco) at 37 °C under 5% CO_2. The 4X test compound (ZM241385, AB928, and target compounds) stock solutions and 4X NECA stock solution were prepared with assay buffer (Hank's buffered saline solution) for use. The test stock solutions were diluted with different gradients for use. The procedure was exemplified by the cAMP functional assay on the A_{2A} receptor: 10,000 cells/well of CHO-K1/ADORA2A/Gα15 were seeded in a 384-well plate in 20 μl of assay buffer. Test compound solutions with different concentrations (2.5 μl) and NECA stock solution (2.5 μl) were added to indicated well of the 384-well plate prepared above and incubated at 37 °C for 30 min. Then, 10 μl of detection reagent (cAMP-d2 and anti-cAMP-Eu3+) was added into each well of the plate and incubated at room temperature for 1 h. The plate was transferred into the PHERA Star for HTRF detection and the data (ratio 665/620) was collected at the wavelength of 665 nm and 620 nm. The inhibition was calculated according to the formula: inhibition (%)=$(R_s–R_0)/(R_1–R_0)\times100\%$, where R_s is the ratio 665/620 value in the presence of target compounds, R_0 is the ratio 665/620 value during the blank assay and R_1 is the ratio 665/620 value in the presence of ZM241385 at a concentration of 1 μM.

4.2.2. A2a AR binding assay

The target compounds were tested to evaluate their affinity for the A_{2A} AR on HEK-293 cell membranes expressing human A_{2A} AR. [^{3}H]-ZM241385 was used as a radioligand. The assay buffer (50 mM Tris-HCl, pH 7.4; 10 mM $MgCl_2$; 1 mM EDTA; 1 μg/ml adenosine deaminase), wash buffer (50 mM Tris-HCl, pH 7.4; 154 mM NaCl), and 0.5% PEI solution were prepared and stored at 4 °C for use. The affinities were tested following the procedure reported by Hu et al[4].

4.2.3 T-cell activation assay

Cryopreserved PBMCs (Allcells) were thawed and recovered in RPMI1640 medium overnight before being used. And compounds to be tested were diluted with DMSO to 100 folds of working concentrations. Then PBMCs were added to 96-well U bottom plate (2.5×10^5 cells per well). To the cells, 2 μl of NECA and 2 μl of each diluted compound (a final concentration of DMSO is 2%) were added. Then, cells were incubated at 37 °C under 5% CO_2 for 1 h. Add 100 μl anti-CD3 (2 μg/ml) and anti-CD28 antibody (2 μg/ml) to each well and cells were cultured for 48 h. After 48 h, supernatants were collected and IL-2 concentration was detected by ELISA.

4.3. Molecular docking

The crystal structure of hA_{2A} AR in complex with antagonist ZM241385 (PDB ID: 5IU4) was retrieved from the Protein Data Bank. The primary sequence of hA_{2B} AR was obtained from the NCBI/UNIPROT online database (www.ncbi.nlm.nih.gov/ protein/P29275.1). Based on the primary sequence, the homology model of hA_{2B} AR was built using the Swiss Model program from a hA_{2A} AR crystal structure as the template (PDB ID: 6PS7)[40] and has been checked using the Ramachandran plot application within Discovery Studio 2017 R2[41]. The molecular docking was performed under the C-DOCKER protocol of Discovery Studio. First, the 3D structure of **7i** was generated and the hydrogenation, dehydration, and CHARMm force field of the protein were executed. Then, the protein was remodelled by removing the antagonist and the 3D molecule of **7i** was placed at the active site for molecular docking. Next, the 2D and 3D predicted binding models of compound **7i** in hA_{2A} AR and hA_{2B} AR were generated.

4.4. Metabolic stability in human and rat liver microsomes

Metabolic stabilities of compounds **7f**, **7i**, and AB928 in liver microsomes were studied with pooled human (male) liver microsomes solution (20 mg/ml) and male Sprague–Dawley rats pooled liver microsomes solution (20 mg/ml) purchased from Research Institute for Liver Diseases (Shanghai) Co. Ltd. Both liver microsomes solutions (140 μl) were diluted by 3948 μl of water and 280 μl of phosphate buffered saline. The assay procedure: 640 μl of diluted liver microsomes solution was added to a solution of compound working solution (16 μl, 25 μM in DMSO) and the mixed solution was incubated at 37 °C for 5 min. Then 160 μl of NADPH generating system was added and take out 100 μl from the mixed solution was added 200 μl of acetonitrile solution to stop the reaction at the set incubation time (0 min, 10 min, 20 min, 30 min, 40 min, 50 min, and 60 min). All stopped reaction solutions were vortex mixed (3 min) and centrifuged (10,000 rpm, 4 °C for 10 min). Then 50 μl of the supernatant was analysed by UPLC-MS/MS system (details of the analytical method see Supporting information).

4.5. Pharmacokinetics assay

Animal experiments were performed according to the institutional ethical guidelines on animal care and approved by the Institute Animal Care and Use Committee at Binzhou Medical University.

The absolute bioavailabilities of synthetic compounds (**7f**, **7i**) were studied in female Bal b/c mice (Jinan Pengyue Experimental Animal Breeding Co., Ltd.). The mice were divided into four groups each having six mice and were collected at crossover time points, with three mice at each point. Pharmacokinetics (PK) was evaluated after a single dose of 30 mg/kg oral gavage (Oral) or 10 mg/kg intravenous (i.v.) administration. After oral administration and i.v. injection, blood samples were obtained from the suborbital veniplex at pre, 15 min, 30 min, 1 h, 2 h, 4 h, 6 h, 8 h, 12 h, 24 h (Oral) and pre, 5 min, 15 min, 30 min, 1 h, 2 h, 4 h, 6 h, 8 h, 12 h, 24 h (i.v.). Approximately 200 μl of blood was collected at each time point. All blood samples were put into plastic microcentrifuge tubes containing Heparin-Na as an anticoagulant. Microcentrifuge tubes with blood samples and anticoagulant were inverted several times for proper mixing of the tube contents to centrifugation for plasma. Plasma samples will be centrifuged at 12,000 rpm for 8 min at 4 °C to obtain the supernatant. The serum sample (25 μl) was treated with acetonitrile (100 μl), after which the mixture was vortex-mixed for 8 min and centrifuged at 10,000 rpm for 10 min at 4 °C. The supernatant layer was collected and then 50 μl of supernatant was injected for the UPLC-MS/MS analysis (details of the analytical method see Supporting information).

Disclosure statement

Ming Liu is an inventor on a Chinese patent application CN113121502A relating to the results of this article. The authors

declare that they have no known competing financial interests or personal relationships that could have appeared to influence the work reported in this paper.

Funding

This work was supported by the Projects of Medical and Health Technology Development Program in Shandong Province [2018WS563], the Scientific Research Foundation of Binzhou Medical University [BY2017KYQD06], and the Shandong Province Higher Educational Youth Innovation Talents Introduction and Cultivation Program-Chemical Biology Research Innovation Team (2019–063).

References

1. Yu F, Zhu C, Xie Q, et al. Adenosine A_{2A} receptor antagonists for cancer immunotherapy. J Med Chem 2020;63:1514–12.
2. Saini A, Patel R, Gaba S, et al. Adenosine receptor antagonists: recent advances and therapeutic perspective. Eur J Med Chem 2022;227:113907.
3. Barresi E, Giacomelli C, Marchetti L, et al. Novel positive allosteric modulators of A_{2B} adenosine receptor acting as bone mineralisation promoters. J Enzyme Inhib Med Chem 2021;36:287–95.
4. Reddy GL, Sarma R, Liu S, et al. Design, synthesis and biological evaluation of novel scaffold benzo[4,5]imidazo [1,2-*a*]pyrazin-1-amine: towards adenosine A_{2A} receptor (A_{2A} AR) antagonist. Eur J Med Chem 2021;210:113040.
5. Betti M, Catarzi D, Varano F, et al. The aminopyridine-3,5-dicarbonitrile core for the design of new non-nucleoside-like agonists of the human adenosine A_{2B} receptor. Eur J Med Chem 2018;150:127–39.
6. Beavis PA, Milenkovski N, Henderson MA, et al. Adenosine receptor 2A blockade increases the efficacy of anti-PD-1 through enhanced antitumor T-cell responses. Cancer Immunol Res 2015;3:506–17.
7. Nascimento DC, Viacava PR, Ferreira RG, et al. Sepsis expands a $CD39^{+}$ plasmablast population that promotes immunosuppression via adenosine-mediated inhibition of macrophage antimicrobial activity. Immunity 2021;54:2024–41.e8.
8. Haskó G, Linden J, Cronstein B, et al. Adenosine receptors: therapeutic aspects for inflammatory and immune diseases. Nat Rev Drug Discov 2008;7:759–70.
9. Dziedzic K, Węgrzyn P, Gałęzowski M, et al. Release of adenosine-induced immunosuppression: comprehensive characterization of dual A_{2A}/A_{2B} receptor antagonist. Int Immunopharmacol 2021;96:107645.
10. Sorrentino C, Miele L, Porta A, et al. Myeloid-derived suppressor cells contribute to A_{2B} adenosine receptor-induced VEGF production and angiogenesis in a mouse melanoma model. Oncotarget 2015;6:27478–89.
11. Hofer F, Di Sario G, Musiu C, et al. A complex metabolic network confers immunosuppressive functions to myeloid-derived suppressor cells (MDSCs) within the tumour microenvironment. Cells 2021;10:2700.
12. Varano F, Catarzi D, Vincenzi F, et al. Structural investigation on thiazolo[5,4-d]pyrimidines to obtain dual-acting blockers of CD73 and adenosine A2A receptor as potential antitumor agents. Bioorg Med Chem Lett 2020;30:127067.
13. Antonioli L, Blandizzi C, Pacher P, et al. Immunity, inflammation and cancer: a leading role for adenosine. Nat Rev Cancer 2013;13:842–57.
14. van Rensburg HDJ, Legoabe LJ, Terre'Blanche G, et al. Synthesis and evaluation of methoxy substituted 2-benzoyl-1-benzofuran derivatives as lead compounds for the development adenosine A1 and/or A2A receptor antagonists. Bioorg Chem 2020;94:103459.
15. Zhang M, Fan S, Zhou X, et al. Design, synthesis and biological evaluation of 2-hydrazinyladenosine derivatives as A_{2A} adenosine receptor ligands. Eur J Med Chem 2019;179:310–24.
16. Renk DR, Skraban M, Bier D, et al. Design, synthesis and biological evaluation of Tozadenant analogues as adenosine A_{2A} receptor ligands. Eur J Med Chem 2021;214:113214.
17. Majellaro M, Jespers W, Crespo A, et al. 3,4-Dihydropyrimidin-2(1*H*)-ones as Antagonists of the human A_{2B} adenosine receptor: optimization, structure-activity relationship studies, and enantiospecific recognition. J Med Chem 2021;64:458–80.
18. Gao Z-G, Jacobson KA. A_{2B} adenosine receptor and cancer. Int J Mol Sci 2019;20:5139.
19. Härter M, Kalthof B, Delbeck M, et al. Novel non-xanthine antagonist of the A_{2B} adenosine receptor: from HTS hit to lead structure. Eur J Med Chem 2019;163:763–78.
20. Lim EA, Bauer TM, Patel MR, et al. A phase I, open-label, multicenter study to assess the safety, pharmacokinetics, and preliminary antitumor activity of AZD4635 both as monotherapy and in combination in patients with advanced solid malignancies: results from prostate cancer patients (NCT02740985). J Clin Oncol 2020;38:5518.
21. Hesk D, Borges S, Dumpit R, et al. Synthesis of 3H, 2H4, and 14 C-MK 3814 (preladenant)). J Labelled Comp Radiopharm 2017;60:194–99.
22. Seitz L, Jin L, Leleti M, et al. Safety, tolerability, and pharmacology of AB928, a novel dual adenosine receptor antagonist, in a randomized, phase 1 study in healthy volunteers. Invest New Drugs 2019;37:711–21.
23. Nunez F, Taura J, Camacho J, et al. PBF509, an adenosine A_{2A} receptor antagonist with efficacy in rodent models of movement disorders. Front Pharmacol 2018;9:120.
24. Caulkett PWR, Jones G, McPartlin M, et al. Adenine isosteres with bridgehead nitrogen. Part 1. Two independent syntheses of the [1,2,4]triazolo[1,5-*a*][1,3,5]triazine ring system leading to a range of substituents in the 2, 5 and 7 positions. J Chem Soc Perk Trans 1995;1:801–08.
25. Iannone R, Miele L, Maiolino P, et al. Adenosine limits the therapeutic effectiveness of anti-CTLA4 mAb in a mouse melanoma model. Am J Cancer Res 2014;4:172–81.
26. Jaakola V-P, Griffith MT, Hanson MA, et al. The 2.6 angstrom crystal structure of a human A_{2A} adenosine receptor bound to an antagonist. Science 2008;322:1211–17.
27. Weinert T, Olieric N, Cheng R, et al. Serial millisecond crystallography for routine room-temperature structure determination at synchrotrons. Nat Commun 2017;8:542.
28. Duroux R, Renault N, Cuelho JE, et al. Design, synthesis and evaluation of 2-aryl benzoxazoles as promising hit for the A_{2A} receptor. J Enzyme Inhib Med Chem 2017;32:850–64.
29. Załuski M, Schabikowski J, Jaśko P, et al. 8-Benzylaminoxanthine scaffold variations for selective ligands

acting on adenosine A_{2A} receptors. Design, synthesis and biological evaluation. Bioorg Chem 2020;101:104033.
30. Bamford SJ, Gillespie RJ, Todd RS. Triazolo [4, 5-*d*] pyramidine derivatives, their preparation, and use as purine receptor antagonists for treating movement disorders and other diseases, Patent WO2009156737; 2009.
31. Sabnis RW. Combination therapy comprising A_{2A}/A_{2B} and PD-1/PD-L1 inhibitors for treating cancer. ACS Med Chem Lett 2021;12:1216–17.
32. Chandrasekaran B, Samarneh S, Jaber AM, et al. Therapeutic potentials of A_{2B} adenosine receptor ligands: current status and perspectives. Curr Pharm Design 2019;25:2741–71.
33. Beatty J, Debien L, Jeffrey J, et al. Azolopyrimidine for the treatment of cancer-related disorders. 2019; US10399962.
34. Bobowska A, Galezowski M, Nowak M, et al. Preparation of imidazo[1,2-*a*]pyrazines as adenosine A_{2A} receptor modulators for the treatment of various diseases. 2019; WO2019002606.
35. Hoang G, Wang X, Carlsen PN, et al. Preparation of pyrazolo- and triazolo-pyrazine derivatives as adenosine receptors A_{2A}/A_{2B} inhibitors. 2020; US20200031835.
36. Wang X, Carlsen PN, He C, et al. Pyrrole tricyclic compounds as A_{2A} and A_{2B} inhibitors and their preparation. 2019; US20190337957.
37. Wang Y, Xu H, Wang H, et al. Design, synthesis, and biological activity studies of istradefylline derivatives based on adenine as A_{2A} receptor antagonists. ACS Omega 2021;6: 4386–94.
38. Ondrackova P, Kovaru H, Kovaru F, et al. The effect of adenosine on pro-inflammatory cytokine production by porcine T cells. Vet Immunol Immunopathol 2012;145: 332–39.
39. Cong W, Sun Y, Sun Y-F, et al. Trifluoromethyl-substituted 3,5-bis(arylidene)-4-piperidones as potential anti-hepatoma and anti-inflammation agents by inhibiting NF-κB activation. J Enzyme Inhib Med Chem 2021;36:1621–30.
40. Waterhouse A, Bertoni M, Bienert S, et al. SWISS-MODEL: homology modelling of protein structures and complexes. Nucleic Acids Res 2018;46:W296–303.
41. da Silva ACR, Araujo JSC, Pita SSdR, et al. *In silico* development of adenosine A_{2B} receptor antagonists for sickle cell disease. J Biomol Struct Dyn 2021; DOI: 10.1080/07391102.2021.1934121.